A Bayesian approach to explore signal execution mechanisms in programmed cell death.

Michael A. Kochen[1], Carlos F. Lopez[1,2,*]

[1] Department of Biomedical Informatics, Vanderbilt University, Nashville, TN

[2] Department of Biochemistry, Vanderbilt University, Nashville, TN

[*] To whom correspondence should be addressed.

Email: c.lopez@vanderbilt.edu

Abstract

Mathematical models of biochemical reaction networks are central to the exploration of network dynamics and bridge the gap between experimental measurements and mechanistic interpretations. However, model parameters are often not available and sparse experimental data leads to challenges in model calibration and parameter estimation. This can in turn lead to inaccurate mechanistic interpretations of experimental data and generate poorly conceived hypotheses for experimental validation. To address this challenge, we evaluate whether a Bayesian probability-based approach can be used to qualitatively explore biochemical network execution mechanisms. To test this approach, we explore the parameter space of extrinsic apoptosis to identify the preferred mode of signal execution. Apoptosis signal processing can take place either through a mitochondria independent (Type I) mode or a mitochondria dependent (Type II) mode. We first show that model subnetworks successfully identify the most likely execution mode for a specific concentration of key molecular regulators. We then show that changes in molecular regulator concentrations alter the overall reaction flux through the network shifting modulating signal flow primarily through either a caspase-only pathway or through the mitochondria. Our work thus demonstrates that Bayesian probability approaches can be used to explore the dynamic behavior of model biochemical systems even with missing or sparse data.

Introduction

Emergent cellular behaviors from complex biochemical network processes are difficult to characterize due to the complex interplay between system components and their interactions [1, 2, 3]. Mathematical models of biochemical processes have evolved alongside experimental measurements to explain observed cellular behaviors and guide hypothesis construction for further testing [4, 5]. Models of biochemical reaction networks are typically based on the Mass-Action kinetics formalism and built to represent known pathway mechanics with knowledge garnered from years or even decades of experimentation [6, 7]. Although these models have yielded important predictions and insights about biochemical network processes, they also depend on kinetic rate parameters and protein concentrations that are often poorly characterized or simply unavailable. A typical work-around is to employ model calibration methods to estimate suitable parameters values via optimization to protein concentration time-course data, which is often scarce [8, 9, 10]. It has also been shown that vector-based methods can find multiple parameter sets whereby models agree with experimental data, based on goodness-of-fit metrics, but the dynamics of the network can exhibit significantly different execution modes [7, 9]. This poses a challenge for the study of dynamic network processes as the mode of signal execution can be highly dependent on a specific parameter set and could in turn lead to inadequate model-based interpretation. Therefore, an approach that can enable researchers to explore the execution mechanisms of a biochemical process from a probabilistic perspective, constrained only by available data, would facilitate a rigorous exploration of network dynamics and accelerate the generation of testable mechanistic hypotheses [11].

In this work, we explore whether a Bayesian probability approach can identify network execution modes in extrinsic apoptosis restricted only by experimental observations. Two execution modes have been identified for extrinsic apoptosis signaling: a mitochondria independent (Type I) mode, whereby initiator caspases directly activate effector caspases and induce cell death, and a mitochondria dependent (Type II) mode whereby initiator caspases engage the Bcl-2 family of proteins, which eventually lead to effector caspase activation (see Box 1 for biology details). Most mammalian cells execute apoptosis via the Type II mechanism, yet the Type I mechanism plays a central role in specific cell types, particularly certain types of lymphocytes [12]. A significant body of experimental and modeling work has identified key regulators for Type I vs Type II execution (see Box 1). However, it is still unclear how network structure and the interplay among multiple regulators can modulate signal execution for either Type I or Type II modes. A more traditional approach would prescribe intricate and detailed experimental measurements of cellular response to yield the desired data and improve our understanding of signal execution. However, the time and cost associated with such experiments makes it unlikely and at times unfeasible to obtain said data. It is here that we see Bayesian inference approaches as a complementary alternative to experimentation that can provide qualitative insights about signal execution mechanisms, by exploring broad parameter space ranges, subject only to available computer time.

Here we show that a Bayesian parameter exploration approach, constrained by network structure or molecular concentrations, can identify the dominant signal execution modes in a reaction network. Specifically, we demonstrate the dependence of Type I or a Type II cellular apoptosis execution on network structure and chemical-species concentrations. We use Bayesian model evidence as a metric for comparisons of signal flow through different pathways of the network and subnetworks to identify how regulators affect execution modes. We introduce two complementary approaches that can be used in tandem to explore signal execution modulation. We first define a *multimodel exploration method* to explore multiple hypothesis about apoptosis execution by deconstructing an established apoptosis network model into functional subnetworks. We also define a *pathway flux method* to characterize the signal flux through specific network pathways within the complete network. Combined, these two approaches enable us to qualitatively identify key network components and molecular regulator combinations that shed mechanistic insights about apoptosis execution. Our approach is generalizable to other mass-action kinetics-based networks where signal execution modes play important roles in cellular outcomes. The work leverages Nested Sampling algorithm methods to efficiently calculate Bayesian evidence on high performance computing (HPC) platforms, both of which are seldom used in biological applications. In this manner we are able to carry out the necessary calculations to explore parameter space and estimate the model evidence within the timespan of days.

Methods

Apoptosis model and simulations

The base model used in this work is a modified version of the Extrinsic Apoptosis Reaction Model (EARM) from Lopez et al. (EARM v2.1) [7] . The original EARM was simplified to reduce complexity in the number of parameters, but still retains the key features of the network for apoptosis execution. Specifically, we reduced the molecular complexity of mitochondrial outer membrane permeabilization (MOMP) down to a representative set of Bcl-2 proteins that capture the behavior of activators, inhibitors, effectors, and sensitizers. We also eliminated intermediate states for Cytochrome-c and SMAC to streamline effector caspase activation, and w added an explicit FADD molecule, a part of the death-inducing signaling complex (DISC) to achieve a more realistic representation of signal initiation. Overall, EARM v2.1 comprised 16 chemical species at non-zero initial concentrations, 50 total chemical species, 62 reactions, and 62 kinetic parameters. The modified model was recalibrated to recapitulate the time-dependent concentration trajectories of truncated Bid, Smac release from the mitochondria, and cleaved PARP analogous to the approach reported previously [42] (Figure S1). The modified EARM was partitioned into six sub-models, encoded in PySB, and are summarized in Figure 2. All simulations were run using the mass-action kinetics formalism as a system of Ordinary Differential Equations (ODEs) using the VODE integrator in SciPy, within the PySB modeling framework. All data results, representative models, and software are distributed with open-source licensing and can be found in the GitHub repository https://github.com/LoLab-VU/BIND.

Bayesian evidence estimation

Bayesian evidence is the normalizing term in a Bayesian calculation and provides a measure for model comparison with regard to their fit to experimental data. It is expressed as:

$$P(D|M) = \int L(D|\theta, M)\, P(\theta|M)\, d\theta \tag{1}$$

Where M is the model under consideration, D is the experimental data, θ is a specific set of parameter values, $L(D|\theta, M)$ is the likelihood function describing the fit of the data to the model under those parameter values, and $P(\theta|M)$ is the prior distribution of parameters. All evidence estimates were made using the nested sampling method, introduced by Skilling [43]. This method simplifies the evidence calculation by introducing a prior mass element $dX = P(\theta|M)\, d\theta$ that is estimated by $(X_{i-i} - X_i)$ where $X_i = e^{-i/N}$, i is the current iteration of the algorithm, and N is the total number of live points. The evidence is then written as

$$Z = \int_0^1 L\, dX \approx \sum_{i=1} L_i (X_{i-1} - X_i) \tag{2}$$

Initialization of the algorithm is carried out by randomly selecting an initial population of parameter sets (points in parameter space) from the prior distribution, scoring each one with the likelihood function, and ranking them from L_{high} to L_{low}. At each iteration of the algorithm a new set of parameter values is selected and scored. If that score is higher than L_{low}, then it is added to the population, at the appropriate rank, and L_{low} is removed from the population and added to the evidence sum (2).

Nested sampling software

All evidence estimates in this work are calculated with MultiNest, a nested sampling-based algorithm designed for efficient evidence calculation on highly multimodel posterior distributions [44, 45]. MultiNest works by clustering the live points (population of parameter sets) and enclosing them in ellipsoids at each iteration. The enclosed space then constitutes a reduced space of admissible parameter sets. This lowers the probability of sampling from low likelihood areas and evaluating points that will only be discarded. The evidence estimate is accompanied by an estimate of the evidence error. The algorithm terminates when the presumed contribution of the highest likelihood member of the current set of live points, $L_{high}X_i$ is below a threshold. Here, we use a threshold of 0.0001 and a population size and 16,000 unless otherwise noted. See [44, 45], for more details on the MultiNest algorithm. We use MultiNest with the Python wrapper PyMultiNest [46], which facilitates the integration with PySB into the parameter sampling pipeline.

Multimodel exploration analysis.

To explore multiple hypotheses for signal execution under different biochemical network structures, we carried out an analysis inspired in the multi-model inference approach [47, 48]. We broke down the EARM network into six subnetworks and tested each across increasing concentrations of the regulator XIAP for efficacy in achieving apoptosis. We define the proportion of cleaved PARP, relative to total PARP, as a metric for effective apoptosis execution. That is, if all PARP has been cleaved, then apoptosis has been completely achieved. We therefore define an objective function that estimates the amount of cleaved PARP as:

$$Obj_{multimodel} = \frac{cParp}{tParp} \quad (3)$$

where $cParp$ is the amount of PARP that has been cleaved and $tParp$ is the total amount of PARP in the system.

When this objective function is substituted into equation (1) in place of the likelihood function, the evidence calculation produces an expected value, an average over the chosen prior parameter range for the proportion of PARP that has been cleaved. In this work we compare the expected values for different subnetworks, pathways, and regulatory conditions only in qualitative terms and as a relative measure of fit to an outcome represented by the objective function.

Pathway flux analysis.

We also explored the effect of molecular regulators of Type I vs Type II execution relative to the apoptosis signal flux through the network as we have done in previous work [49]. Briefly, signal flux is defined as the chemical reaction flux in units of molecules per unit time, that traverses through a given pathway. In the apoptosis network there are two potential pathways that can lead to Caspase-3 activation and subsequently PARP cleavage. In the direct caspase pathway initiator caspases represented here as "Caspase-8" directly cleave and activate the effector caspases represented here as "Caspase-3". By contrast, in the mitochondrial pathway, effector caspases are activated via the apoptosome, and are dependent on mitochondrial outer membrane permeabilization (MOMP). Therefore, the dominant pathway responsible for Caspase-3 activation defines the route of the signal. To estimate the flux through the Type I vs Type II pathway, we define an objective function as:

$$Obj_{pathway} = \sum_{t=0}^{T} \frac{\sum_0^t C3_{pathway}}{\sum_0^t C3_{total}} \times (cParp_t - cParp_{t-1}) \quad (4)$$

where t represents time in seconds, $\sum_0^t C3_{pathway}$ is the amount of Caspase-3 activated via the target pathway up to time t, $\sum_0^t C3_{total}$ is the total Caspase-3 activated up to time t, and $\sum_0^t C3_{caspase} / \sum_0^t C3_{total}$ is the proportion of activated Caspase-3 that was produced via the target pathway up to time t. $(cParp_t - cParp_{t-1})$ is the total PARP that has been cleaved, and activated, by Caspase-3 from time $t-1$ to time t.Thus, at any given time t we can estimate the amount of Caspase-3 that has been activated through a specific pathway. Multiplication of these two terms returns an estimate for the amount of PARP cleaved via the specific pathway at time t. Summing over T then returns an estimate for the total apoptosis signal flowing through the target pathway. Like the PARP cleavage objective function, the signal flux objective substituted into equation (1) produces an estimate of the average flux over a defined prior distribution. We estimated this quantity over increasing concentrations of the of the molecular regulator XIAP, but also at high and low levels of the DISC components FADD and Caspase-8. The total signal flux was estimated by summing the evidence estimates for the flux through either the direct caspase or mitochondrial pathway.

Parameter ranges and initial conditions.

The prior distribution takes the form of a set of parameter ranges, one for each reaction rate parameter. The chosen ranges span four orders of magnitude around generic reaction rates

deemed plausible [4] and are specific to the type of reaction taking place. The ranges of reaction rate parameters, in Log_{10} space, are 1st order forward: [-4.0, 0.0], 2nd order forward: [-8.0, -4.0], 1st order reverse: [-4.0, 0.0], catalysis: [-1.0, 3.0]. These ranges were also used in calibration of the base model. Initial conditions were either gleaned from the literature [50, 51] or taken from a previous model of extrinsic apoptosis [7]. Because the baseline model was designed to concur with Type II apoptotic data (see above), literature derived initial conditions were based on Type II Jurkat or Hela cell lines (Table S1).

Bayes factors.

Evidence estimates are often used to select between two competing models by calculating the Bayes factor (i.e. the ratio of their evidence values). This provides a measure of confidence for choosing one model over another. We can likewise use trends in evidence values to produce trends in Bayes factors that provide additional insights into the dynamical relationship between pathways. To facilitate construction of Bayes factor trends with a continuous and symmetric range, the we calculated Bayes factors as:

$$Bf = \begin{cases} -\frac{Z_2}{Z_1} + 1 \;\; if \; Z_1 < \; Z_2 \\ \frac{Z_1}{Z_2} - 1 \;\; if \; Z_1 > \; Z_2 \end{cases}$$

where Z_1 and Z_2 are the evidence estimates for two pathways under comparison.

Computational resources

Because of the high computational workload necessary for this analysis, a wide range of computational resources were used. The bulk of the work was done on the ACCRE cluster at Vanderbilt University which has more than 600 compute nodes running Intel Xeon processors and a Linux OS. As many as 300 evidence estimates were run in parallel on this system. Additional resources included two local servers, also running Intel processors and a Linux OS, as well as a small local four node cluster running Linux and AMD Ryzen 1700 processors. A detailed breakdown of CPU time can be found in the results section. In all evidence estimates for 14 different networks/initial conditions were made across the range of XIAP concentrations. We estimate all 14 runs would take ~9 days each on a typical university server with 32 cores/64 threads.

Results

Overview: A Bayesian evidence approach to explore mechanistic hypotheses.
Our overarching goal is to understand the mechanisms and dynamics of biochemical networks responsible for cellular commitment to fate, given incomplete or unavailable data. We take a Bayesian probability approach to study model subnetworks and specific model pathways as summarized schematically in Figure 1 to estimate the evidence for signaling execution mechanisms given a set of experimental data and existing priors.

In the *Multimodel Exploration Analysis* (Figure 1, left path), the network model is deconstructed into biologically relevant subnetworks and the probability of each subnetwork achieving apoptosis, under various regulatory conditions, is estimated via Bayesian evidence. This differs from traditional model selection and multimodel inference applications where models are typically ranked based on their fit to experimental data and high-ranking models may be averaged to obtain a composite model [47, 48, 52, 53, 54, 55]. Here, we already have a model that captures key features of programmed cell death execution. Instead, we use the differences in evidence to construct a composite picture of mechanistic evidence for apoptosis execution. To achieve this, we first tailor the objective function to represent signal execution strength, as measured by cleaved PARP concentration at the end of the simulation. The evidence derived from this objective function therefore describes the likelihood that the signal is effectively transmitted through the (sub)network. It should be noted that Bayesian evidence inherently incorporates model complexity as the objectives are integrated over normalized prior distributions [44, 52, 56]. As we will see, comparison of changes in signal strength through relevant subnetworks allows inferences to be made on the effect of the perturbed network regulator as well as various network components on the overall dynamics of the system. We focus primarily on understanding how Bayesian evidence for the caspase pathway compares to that of the complete network as these are most relevant for the analysis of Type I/II execution modes. This analysis will inform on how network components contribute to overall signal execution and provide mechanistic insights about the sensitivity of PARP cleavage to subnetwork components.

In the *Pathway Flux Analysis* (Figure 1, right path), we retain the complete network structure but instead tailor the objective functions to measure biochemical reaction flux, as described in the Methods section, through either the direct caspase or mitochondrial pathways. We primarily consider the influence of the apoptosis inhibitor XIAP on regulatory dynamics and phenotypic fate but also consider the regulatory effect of the death inducing signaling complex (DISC) and the anti-apoptotic protein Bcl-2, all of which have been found to be relevant to Type I vs Type II execution in different cell types [13, 14]. This analysis will inform on how molecular regulators modulate biochemical flux through the network and their influence on apoptosis completion as measured by PARP cleavage.

Decomposition of the extrinsic apoptosis network and reductive analysis of the effects of XIAP
To investigate the effect of network substructures on apoptosis signaling, we build a composite description of system dynamics by observing variations in signal throughput, represented by evidence values for PARP cleavage, between subnetworks (Figure 2A-F) relative to changes in

267 regulatory conditions. We consider relative changes in the evidence values as the number of
268 XIAP molecules is increased where a higher evidence value indicates a stronger signal over the
269 prior range of parameter values. XIAP was varied from 0 to 200,000 molecules per cell in
270 increments of 250 to explore how changes in XIAP affect the likelihood of apoptosis execution.
271 For subnetworks that include the mitochondrial pathway, Bcl-2 (an anti-apoptotic) was reduced
272 or eliminated, to explore Type I vs Type II activity independent of inhibitors that could confound
273 signal throughput, and more closely simulate a cells that is "primed" for death [56]. All other
274 initial values were fixed at the levels shown in supplementary Table S1. In the absence of XIAP
275 all six subnetworks have evidence estimates greater than 0.98, (Figure 2 A: 0.993, B: 0.998, C:
276 0.992, D: 0.981, E: 0.998, F: 0.981, Table S2) indicating that they can all capture a biological
277 process that leads to PARP cleavage across the allowed range of parameters, as expected. We
278 further explore how XIAP can modulate Type I/II apoptosis execution for a chosen subnetwork .

279 The results in Jost et al. [14] imply that the cellular level of XIAP determines the preferred
280 apoptosis pathway with higher levels specific to Type II cells and lower levels specific to Type I.
281 To hypothesize a possible mechanistic explanation for this behavior we compared the
282 computed the Bayesian evidence values, over increasing concentrations of XIAP, for the direct
283 caspase activation network against both the complete network and the mitochondrial network
284 (Figures 2A and G green; 2E and G orange; 2F G blue respectively). . This mimics reported
285 experimental strategies to study Type I/II phenotypes and allows us to gauge the effect of XIAP
286 on networks with and without a mitochondrial component [13, 35].

287 As XIAP levels increase we see differential effects on all subnetworks in the form of diverging
288 evidence estimates, indicating differences in the efficacy of XIAP induced apoptotic inhibition.
289 The evidence values for the isolated caspase pathway (Figure 2G green) diverges from the
290 complete network (Figure 2G orange) and mitochondrial pathway (Figure 2 blue) showing a
291 steeper initial decline that diminishes as XIAP continues to increase. PARP cleavage evidence
292 values for the caspase pathway falls to 0.5 at an XIAP level of roughly 32,000. However, the
293 complete network and mitochondrial pathways require XIAP levels nearly threefold higher with
294 the evidence value reaching 0.5 at around 92,000 and 95,000 respectively.

295 Because the direct caspase activation pathway (Figures 2G green) is representative of the Type I
296 phenotype, the disproportionate drop in its evidence of PARP cleavage as XIAP concentration
297 increases is consistent with experimental evidence showing XIAP-induced transition from a
298 Type I to a Type II execution mode [14]. The complete network, containing the full
299 mitochondrial subnetwork, and mitochondrial only pathway are also affected by XIAP but
300 exhibits resistance to its anti-apoptotic effects, a difference that is most prominent at
301 moderate levels of the inhibitor. This suggests a growing dependence on mitochondrial
302 amplification for effective apoptosis as XIAP increases from low to moderate levels. At higher
303 levels of XIAP the evidence values for the caspase pathway level off and the gap between it and
304 the two mitochondrial containing networks narrows. The disproportionate effect of XIAP
305 inhibition of apoptosis on the caspase pathway suggests that the mechanism for XIAP induced
306 transition to a Type II pathway can be attributed to differential inhibition of the apoptotic signal
307 through the isolated caspase pathway vs a network with mitochondrial involvement.

308 We note here that the small differences in evidence values between the various networks
309 should not be surprising since every subnetwork being considered is capable of carrying
310 apoptosis to completion, as measured by PARP cleavage. Thus, we should not expect evidence
311 differences that would rule out any model under a model selection criterion. The log-evidence
312 version of Figure 2G along with estimated errors generated by MultiNest are displayed in Figure
313 S2.

314 The next two highest trends in evidence values after that of the direct caspase network (Figure
315 2G green) belong to the networks representing direct caspase activation plus mitochondrial
316 activation and mitochondrial activation alone (Figures 2G purple and 2G brown). For most of
317 the range with XIAP below 100,000 these two networks have largely overlapping evidence
318 trajectories, despite the fact that the former has twice as many paths carrying the apoptotic
319 signal. Near an XIAP level of 100,000 the two trends diverge as the decrease in evidence values
320 for the mitochondrial activation only network accelerates. This could be explained by XIAP
321 overwhelming the Apoptosome at these higher levels. The apoptosome is an apoptosis inducing
322 complex (via Caspase-3 cleavage) consisting of Cytochrome C, APAF-1, and Caspase-9, and is an
323 inhibitory target of XIAP. As XIAP increases past 125,000 the mitochondrial activation only
324 evidence values fall below even the solo direct caspase values, possibly due to the two-pronged
325 inhibitory action of XIAP at both the Apoptosome and Caspase-3. An interesting observation
326 here is that the addition of the direct caspase pathway to the mitochondrial activation pathway
327 does not appear to increase the likelihood of achieving apoptosis for lower values of XIAP.

328 Evidence values for the network representing direct caspase activation plus mitochondrial
329 inhibition of XIAP are in red in Figure 2G. Below an XIAP level of 100,000 these values are
330 consistently above the evidence values for the network of the direct caspase plus mitochondrial
331 activation. Note that while direct caspase activation does not appear to increase the likelihood
332 of achieving apoptosis when added to the mitochondrial activation pathway (Figure 2G purple)
333 the amplification of the direct caspase activation via mitochondrial inhibition of XIAP leads to a
334 higher likelihood than solo activation through the mitochondria. This suggests the possibility
335 that the primary mechanism for mitochondrial apoptotic signal amplification, under some
336 conditions, may be inhibition of XIAP, with direct signal transduction a secondary mechanism.
337 Above an XIAP level of 100,000, the direct caspase with XIAP inhibition values drop to levels
338 roughly in line with the values for direct caspase activation plus mitochondrial activation,
339 possibly due to the fact that Smac, the mitochondrial export that inhibits XIAP, is also set to
340 100,000 molecules per cell. Both, however, remain more likely to attain apoptosis than direct
341 caspase activation alone.

342 The two subnetworks with the highest evidence values for apoptotic signal execution are the
343 complete network and the isolated mitochondrial pathway (Figures 2E orange and 2F blue). As
344 previously mentioned, both of these networks contain the full mitochondrial pathway implying
345 that this pathway supports resistance to XIAP inhibition of apoptosis. Between XIAP levels of 0
346 to 100,000 the two trends track very closely, with the mitochondrial only pathway showing a
347 slight but consistent advantage for apoptosis execution. The average difference between an
348 XIAP level of 20,000 and 80,000 is roughly 0.014, meaning we expect the average PARP
349 cleavage to favor the mitochondrial only pathway by about 1.4 percentage points, which may
350 seem unremarkable. Context matters however, and the context here is that the complete

351 network has potentially twice the bandwidth for the apoptotic signal, namely the addition of
352 the more direct caspase pathway. Together, this raises the possibility that under some
353 conditions the caspase pathway is not a pathway but a sink for the apoptotic signal. In such a
354 scenario, the signal through the caspase pathway would get lost as Caspase-3 is degraded by
355 XIAP. Not until the signal through the mitochondrial pathway begins inhibiting XIAP could the
356 signal proceed. Around the 100,000 level of XIAP the evidence trend for the mitochondrial
357 pathway crosses below that for the complete network. This could be due to the parity with
358 Smac, components of the Apoptosome, or a combination of the two.

359 **Apoptosis signal strength drives signal route through the network**

360 The results in Scaffidi et al. [13] indicate a strong phenotypic dependence on the strength of the
361 apoptosis signal. Here we examine hypotheses made in that work and the interplay between
362 the DISC and XIAP regulatory axes. We once again increase XIAP from 0 to 200,000 molecules
363 in increments of 250, but this time at a low number of DISC complexes by lowering the initial
364 values of both the scaffold protein FADD and the initiator Caspase-8, from 130,000 to 100
365 molecules per cell. In addition to the Multimodel Exploration Approach used in the previous
366 section, we also use the Pathway Flux Approach using the flux objective function (see
367 Methods). In this way we attain a holistic view of network dynamics that incorporates both,
368 network structure and flux cross-talk from all possible pathways. Additional analysis of caspase
369 and mitochondrial pathway signal flux over a range of values for both XIAP and BCL-2 is
370 displayed in Figure S3 and interpreted in Text S1.

371 Figure 3A displays the PARP cleavage evidence values along with their low DISC counterparts.
372 Two things are immediately apparent. The PARP cleavage evidence values for the caspase
373 pathway at low number of DISC is lower across the entire range of changes in the number of
374 XIAP molecules. The complete network on the other hand shows almost no difference in low
375 DISC conditions at lower values of XIAP. This supports the hypothesis that mitochondrial
376 involvement is necessary to overcome weak DISC formation and that low number of DISC likely
377 constitutes a Type II trait [13].

378 Figures 3B and 3C show evidence values for flux through the caspase pathway and complete
379 network for high and low number of DISC, respectively. At higher DISC values, signal flux
380 through the caspase pathway is consistently higher than the flux through the mitochondrial
381 pathway. At lower DISC values the signal flux through the mitochondrial pathway exceeds the
382 flux through the caspase pathway. Our results shed interesting mechanistic observations in the
383 context of a previously proposed hypothesis stating that mitochondrial activation is
384 downstream of caspase activation in Type I cells and upstream in Type II cells. If a weaker initial
385 apoptosis cue does indeed push the signal through the mitochondrial pathway the initial
386 activation of Caspase-8 would be weak and the amplifying activity of the mitochondria would
387 ramp up the signal before Caspase-8 could directly activate Caspase-3. On the other hand,
388 strong initial activation that pushes the signal through the caspase pathway would have the
389 opposite effect. Also notable is the nearly identical trajectories of the total signal flux through
390 the low and high DISC models. The average difference over the range of XIAP was only 0.011
391 (Table S3). This is consistent with observations that both Type I and Type II cells respond equally
392 well to receptor mediated apoptosis.[13]

393 Overall these results set up three mechanistic explanations for apoptosis execution. On one
394 end, high DISC formation and low XIAP results in the independence of apoptosis from the
395 mitochondrial pathway. This behavior is consistent with Type I cells like the SKW6.4 cell lines
396 [13]. On the other end of the spectrum is the case with low DISC formation (and by construction
397 low Caspase-8 activity) and near complete dependence on the mitochondrial pathway. Such
398 behavior is consistent with Type II cells like Jurkat [13]. In between these two extremes is the
399 case where DISC formation, and subsequent Caspase-8 activation, is high but apoptosis is still
400 dependent on mitochondrial activity. Such behavior is consistent with MCF-7 cell that are
401 known to have traits of both phenotypes [13].

402 **Bayes factor trends and XIAP influence on Type I/II apoptosis phenotype**

403 Model selection methods typically calculate the evidence ratios, or Bayes factors to choose a
404 preferred model and estimate the confidence of that choice [58, 59]. When comparing the
405 changes in the evidence of an outcome as regulatory conditions change, the changes in the
406 evidence ratios can provide additional information about changing network dynamics under
407 regulatory perturbations. To characterize the effect of XIAP on the choice of apoptotic
408 phenotype, Type I or II, we calculated the evidence ratios (Figure 4A), for each value of XIAP
409 between the caspase pathway and both the complete network and mitochondrial pathway
410 with a fully active mitochondrial pathway. In these calculations, the denominator represents
411 the caspase pathway so that higher values favor a need for mitochondrial involvement. An
412 interesting feature of both the complete and mitochondrial evidence ratio trends is the peak
413 and reversal at a moderate level XIAP (Figure 4B). This reflects the initially successful inhibition
414 of the caspase pathway that decelerates relatively quickly as XIAP increases, and a steadier rate
415 of increased inhibition on networks that incorporate the mitochondrial pathway. The ratios
416 peak between 45,000 and 50,000 molecules of XIAP (more than double the value of its target
417 molecule Caspase-3 at 21,000) and represent the optimal level of XIAP for the requirement of
418 the mitochondrial pathway and attainment of a Type II execution. Given the near monotonic
419 decline of the evidence trends of both pathways, representing increasing suppression of
420 apoptosis, the peak and decline in the evidence ratios could represent a shift toward complete
421 apoptotic resistance. Our results therefore complement the observations in Aldridge et al.
422 where a similar outcome was observed experimentally [60].

423 A common technique to study apoptosis is to knockdown Bid, overexpress Bcl-2, or otherwise
424 shut down MOMP induced apoptosis through mitochondrial regulation. This strategy was used
425 in Jost et al. [14] to study the role of XIAP in apoptosis and in the work of Aldridge et al. to
426 explore Type I vs Type II execution in different cell lines [59]. Taking a similar approach, we set
427 Bcl-2 levels to 328,000 molecules per cell, in line with experimental findings [47], to suppress
428 MOMP activity and recreated the evidence and ratios landscapes (Figures 4C and 4D, Table S5).
429 Under these conditions the evidence trend for the mitochondrial pathway drops well below
430 that of the caspase pathway, which is reflected in the Bayes factor trend as a shift into negative
431 values and indicating that the caspase pathway is favored. The evidence trend for the complete
432 network under MOMP inhibition is shifted closer to that for the caspase pathway at higher
433 concentrations of XIAP but the Type II pathway continues to dominate throughout the full
434 range of XIAP. The peak for the associated Bayes factor trend is flattened as the number of XIAP
435 increases, suggesting that increasing XIAP levels are less likely to induce a transition to a Type II

phenotype in a system with an already hampered mitochondrial pathway. We note that complete inhibition of MOMP would result in uninformative mitochondrial pathway evidence values. The evidence trend for the complete network would be indistinguishable from that for the caspase pathway alone and the complete/caspase ratio trend would simply flatline. However, our analysis shows that isolation of active biologically relevant subnetworks and direct comparison under changing molecular regulator conditions using trends in Bayesian evidence enables the extraction of information regarding the pathway interactions and differential network dynamics.

Precision vs computational cost

Increasing the precision of the evidence estimates, and tightening the evidence trendlines, is accomplished by increasing the number of live points in the nested sampling algorithm. The trade-off is an increase in the number of evaluations required to reach the termination of the algorithm and an accompanying increase in total computation time. Figures 5A and 5B display the required number of evaluations for the caspase pathway and complete network at population sizes of 500, 1000, 2000, 4000, 8000, and 16,000, when run with the PARP cleavage objective function. For both models the number of evaluations roughly doubles for every doubling in population size. Of note here is the higher number of required evaluations for the lower parameter model. The caspase pathway has only 22 parameters and required an average of 64,612 evaluations at a population size of 16,000 while the complete network, with its 56 parameters required only 53,652 evaluations, on average (Table S6). Figures 5C and 5D are the average estimated errors calculated by the MultiNest algorithm over each population size for the caspase and complete networks respectively. As expected, error estimates fall roughly as $n^{-1/2}$ [61], signifying clear diminishing returns as the number of live points is increased. The average CPU process times, as estimated by Python's `time.clock()` method, are given in Figures 5E and 5F for the caspase and complete networks respectively. Despite the greater number of required evaluations for the caspase network the average clock times for the complete network is significantly higher. At a population of 16,000 the caspase network had an average clock time of 11,964 seconds compared to 76,981 for the complete network. The difference is due to the greater simulation time for the much larger complete model. Ultimately, the choice of population size for the methods we have laid out here will depend on the networks to be compared, the objective function, and how well the evidence trends must be resolved in order to make inferences about network dynamics. For example, at a population size of 500 the evidence trend for the caspase pathway is clearly discernable from the mitochondrial pathway and the complete network, but the latter two are largely overlapping (Figure S4A). At higher population levels, however, two distinct mitochondrial and complete trends become apparent (Figure SK). If Bayes factor trends are desired then the choice of population size must take into consideration the amplification of the noise from both trends (see Figures S4(B, D, F, H, J, L) for complete/caspase Bayes factor trends).

Discussion

Characterizing information flow in biological networks, the interactions between various pathways or network components, and shifts in phenotype upon regulatory perturbations is standing challenge in molecular biology. Although comparative analysis of signal flow within a network is possible with current computational methods, the dependence of physicochemical models on unknown parameters makes the computational examination of each network component highly dependent on costly experimentation.

To take advantage of the enormous amount of existing knowledge encoded in these physicochemical networks without the dependence on explicit parameter values we take a probabilistic approach to the exploration of changes in network dynamics. By integrating an objective function that represents a simulated outcome over parameter distributions we obtain the likelihood of attaining that outcome given the available information about the signaling pathways. Qualitative exploration of network behavior for various in silico experimental setups and regulatory conditions are then attainable without explicit knowledge of every parameter value. We demonstrate the utility of the method when applied to the regulation of extrinsic apoptosis. Networks that incorporate an active mitochondrial pathway displayed a higher resistance to apoptotic inhibition from increasing levels of XIAP, consistent with experimental evidence that XIAP induces a Type II phenotype [14]. Also in line with experimental evidence [13] are the results that suggest low/high signal initiation is consistent with Type II/I phenotype respectively and that both types achieve apoptosis equally well.

A potential limitation of a Bayesian approach to study network dynamics could be the computational cost. A number of factors affect the run time of the algorithm including size of the model, the objective function, and the desired precision. Fortunately, reducing the resolution (the number of sets of initial values for which an evidence value is estimated) and the precision (the population size) can drastically reduce the cost and in many cases the method will still be viable. One aspect of the method that is severely restrictive is the number of model components that can be varied in the same run since the computational cost increases exponentially with each additional variable. Reasonable parameter ranges must also be chosen. Information regarding the parameters can be incorporated into the evidence calculations by adjusting the range and shape of the priors. Here we used generic but biologically plausible ranges with uniform distributions and produced results that were qualitatively consistent with previous experimental results. We note, however, that our results make mechanistic inferences from model experiments given existing data over a period of weeks rather than the months or years that would be required to attain this information with experimental approaches. Our results therefore support Bayesian approaches as a suitable complement to experimentation and a shift from purely deterministic models with a single optimum parameter set to a probabilistic understanding of mechanistic models of cellular processes.

Conclusions

In this paper we have developed a probabilistic approach to the qualitative analysis of the network dynamics of physicochemical models. It is designed to incorporate all available knowledge of the reaction topology, and the parameters on that topology, and calculate the likelihood of achieving an outcome of interest. Inferences on network dynamics are then made by repeating this calculation under changing regulatory conditions and various in silico experiments. We tested the method against a model of the extrinsic apoptosis system and produced results that were consistent with several lines of experimental research. To our knowledge this is the first attempt at a probabilistic analysis of network dynamics for physicochemical models. We believe this method will prove valuable for the large-scale exploration of those dynamics, particularly when parameter knowledge and data are scarce.

Acknowledgements

This work was supported by the NIH NCI U01CA215845 (CFL), as well as NSF MCB 1411482 (CFL) We thank the Incyte-Vanderbilt Alliance (CFL) for their support of this project. We also thank the Advanced Computing Center for Research and Education (ACCRE) for computational resources and support needed to complete this work. Finally, we extend our thanks to Dr Blake Wilson for his effort in reviewing this work and providing feedback.

535 ## References

536 1. Bhalla US, Iyengar R. Emergent Properties of Networks of Biological Signaling Pathways.
537 Science. 1999 Jan 15;283(5400):381–7.

538 2. Loscalzo J, Barabasi A-L. Systems biology and the future of medicine. Wiley
539 Interdisciplinary Reviews: Systems Biology and Medicine. 2011;3(6):619–27.

540 3. Kitano H. Computational systems biology. Nature. 2002 Nov;420(6912):206–10.

541 4. Aldridge BB, Burke JM, Lauffenburger DA, Sorger PK. Physicochemical modelling of cell
542 signalling pathways. Nat Cell Biol. 2006 Nov;8(11):1195–203.

543 5. Le Novère N. Quantitative and logic modelling of molecular and gene networks. Nature
544 Reviews Genetics. 2015 Mar;16(3):146–58.

545 6. Albeck JG, Burke JM, Spencer SL, Lauffenburger DA, Sorger PK. Modeling a Snap-Action,
546 Variable-Delay Switch Controlling Extrinsic Cell Death. PLOS Biology. 2008 Dec
547 2;6(12):e299.

548 7. Lopez CF, Muhlich JL, Bachman JA, Sorger PK. Programming biological models in Python
549 using PySB. Molecular Systems Biology. 2013 Jan 1;9(1):646.

550 8. Riel V, A.w N. Dynamic modelling and analysis of biochemical networks: mechanism-
551 based models and model-based experiments. Brief Bioinform. 2006 Dec 1;7(4):364–74.

552 9. Shockley EM, Vrugt JA, Lopez CF. PyDREAM: high-dimensional parameter inference for
553 biological models in python. Bioinformatics. 2018 Feb 15;34(4):695–7.

554 10. Mitra ED, Suderman R, Colvin J, Ionkov A, Hu A, Sauro HM, et al. PyBioNetFit and the
555 Biological Property Specification Language. arXiv:190307750 [q-bio] [Internet]. 2019 Mar
556 18 [cited 2019 Nov 1]; Available from: http://arxiv.org/abs/1903.07750

557 11. Wrede F, Hellander A. Smart computational exploration of stochastic gene regulatory
558 network models using human-in-the-loop semi-supervised learning. bioRxiv. 2018 Dec
559 8;490623.

560 12. Scaffidi C, Schmitz I, Zha J, Korsmeyer SJ, Krammer PH, Peter ME. Differential Modulation
561 of Apoptosis Sensitivity in CD95 Type I and Type II Cells. J Biol Chem. 1999 Aug
562 6;274(32):22532–8.

563 13. Scaffidi C, Fulda S, Srinivasan A, Friesen C, Li F, Tomaselli KJ, et al. Two CD95 (APO-1/Fas)
564 signaling pathways. The EMBO Journal. 1998 Mar 16;17(6):1675–87.

565 14. Jost PJ, Grabow S, Gray D, McKenzie MD, Nachbur U, Huang DCS, et al. XIAP discriminates
566 between type I and type II FAS-induced apoptosis. Nature. 2009 Aug;460(7258):1035–9.

567 15. Ashkenazi A, Dixit VM. Death Receptors: Signaling and Modulation. Science. 1998 Aug
568 28;281(5381):1305–8.

569 16. Boldin MP, Varfolomeev EE, Pancer Z, Mett IL, Camonis JH, Wallach D. A Novel Protein
570 That Interacts with the Death Domain of Fas/APO1 Contains a Sequence Motif Related to
571 the Death Domain. J Biol Chem. 1995 Apr 7;270(14):7795–8.

572 17. Kischkel FC, Lawrence DA, Chuntharapai A, Schow P, Kim KJ, Ashkenazi A. Apo2L/TRAIL-
573 Dependent Recruitment of Endogenous FADD and Caspase-8 to Death Receptors 4 and 5.
574 Immunity. 2000 Jun 1;12(6):611–20.

575 18. Sprick MR, Weigand MA, Rieser E, Rauch CT, Juo P, Blenis J, et al. FADD/MORT1 and
576 Caspase-8 Are Recruited to TRAIL Receptors 1 and 2 and Are Essential for Apoptosis
577 Mediated by TRAIL Receptor 2. Immunity. 2000 Jun 1;12(6):599–609.

578 19. Krueger A, Schmitz I, Baumann S, Krammer PH, Kirchhoff S. Cellular FLICE-inhibitory
579 Protein Splice Variants Inhibit Different Steps of Caspase-8 Activation at the CD95 Death-
580 inducing Signaling Complex. J Biol Chem. 2001 Jun 8;276(23):20633–40.

581 20. Salvesen GS, Dixit VM. Caspase activation: The induced-proximity model. PNAS. 1999 Sep
582 28;96(20):10964–7.

583 21. Martin DA, Siegel RM, Zheng L, Lenardo MJ. Membrane Oligomerization and Cleavage
584 Activates the Caspase-8 (FLICE/MACHα1) Death Signal. J Biol Chem. 1998 Feb
585 20;273(8):4345–9.

586 22. Boatright KM, Salvesen GS. Mechanisms of caspase activation. Current Opinion in Cell
587 Biology. 2003 Dec 1;15(6):725–31.

588 23. Stennicke HR, Jürgensmeier JM, Shin H, Deveraux Q, Wolf BB, Yang X, et al. Pro-caspase-3
589 Is a Major Physiologic Target of Caspase-8. J Biol Chem. 1998 Oct 16;273(42):27084–90.

590 24. Li H, Zhu H, Xu C, Yuan J. Cleavage of BID by Caspase 8 Mediates the Mitochondrial
591 Damage in the Fas Pathway of Apoptosis. Cell. 1998 Aug 21;94(4):491–501.

592 25. Luo X, Budihardjo I, Zou H, Slaughter C, Wang X. Bid, a Bcl2 Interacting Protein, Mediates
593 Cytochrome c Release from Mitochondria in Response to Activation of Cell Surface Death
594 Receptors. Cell. 1998 Aug 21;94(4):481–90.

595 26. Desagher S, Osen-Sand A, Nichols A, Eskes R, Montessuit S, Lauper S, et al. Bid-induced
596 Conformational Change of Bax Is Responsible for Mitochondrial Cytochrome c Release
597 during Apoptosis. The Journal of Cell Biology. 1999 Mar 8;144(5):891–901.

598 27. Kelekar A, Thompson CB. Bcl-2-family proteins: the role of the BH3 domain in apoptosis.
599 Trends in Cell Biology. 1998 Aug 1;8(8):324–30.

600 28. Oltval ZN, Milliman CL, Korsmeyer SJ. Bcl-2 heterodimerizes in vivo with a conserved
601 homolog, Bax, that accelerates programed cell death. Cell. 1993 Aug 27;74(4):609–19.

602 29. Leber B, Lin J, Andrews DW. Embedded together: The life and death consequences of
603 interaction of the Bcl-2 family with membranes. Apoptosis. 2007 May 1;12(5):897–911.

604 30. Letai A, Bassik MC, Walensky LD, Sorcinelli MD, Weiler S, Korsmeyer SJ. Distinct BH3
605 domains either sensitize or activate mitochondrial apoptosis, serving as prototype cancer
606 therapeutics. Cancer Cell. 2002 Sep 1;2(3):183–92.

607 31. Yang E, Zha J, Jockel J, Boise LH, Thompson CB, Korsmeyer SJ. Bad, a heterodimeric
608 partner for Bcl-xL and Bcl-2, displaces bax and promotes cell death. Cell. 1995 Jan
609 27;80(2):285–91.

610 32. Kale J, Osterlund EJ, Andrews DW. BCL-2 family proteins: changing partners in the dance
611 towards death. Cell Death Differ. 2018 Jan;25(1):65–80.

612 33. Tewari M, Quan LT, O'Rourke K, Desnoyers S, Zeng Z, Beidler DR, et al. Yama/CPP32β, a
613 mammalian homolog of CED-3, is a CrmA-inhibitable protease that cleaves the death
614 substrate poly(ADP-ribose) polymerase. Cell. 1995 Jun 2;81(5):801–9.

615 34. Nicholson DW, Ali A, Thornberry NA, Vaillancourt JP, Ding CK, Gallant M, et al.
616 Identification and inhibition of the ICE/CED-3 protease necessary for mammalian
617 apoptosis. Nature. 1995 Jul;376(6535):37–43.

618 35. Jost PJ, Grabow S, Gray D, McKenzie MD, Nachbur U, Huang DCS, et al. XIAP discriminates
619 between type I and type II FAS-induced apoptosis. Nature. 2009 Aug;460(7258):1035–9.

620 36. Huang Y, Park YC, Rich RL, Segal D, Myszka DG, Wu H. Structural Basis of Caspase
621 Inhibition by XIAP: Differential Roles of the Linker versus the BIR Domain. Cell. 2001 Mar
622 9;104(5):781–90.

623 37. Suzuki Y, Nakabayashi Y, Takahashi R. Ubiquitin-protein ligase activity of X-linked
624 inhibitor of apoptosis protein promotes proteasomal degradation of caspase-3 and
625 enhances its anti-apoptotic effect in Fas-induced cell death. PNAS. 2001 Jul
626 17;98(15):8662–7.

627 38. Shiozaki EN, Chai J, Rigotti DJ, Riedl SJ, Li P, Srinivasula SM, et al. Mechanism of XIAP-
628 Mediated Inhibition of Caspase-9. Molecular Cell. 2003 Feb 1;11(2):519–27.

629 39. Zou H, Li Y, Liu X, Wang X. An APAF-1·Cytochrome c Multimeric Complex Is a Functional
630 Apoptosome That Activates Procaspase-9. J Biol Chem. 1999 Apr 23;274(17):11549–56.

631 40. Adrain C, Creagh EM, Martin SJ. Apoptosis-associated release of Smac/DIABLO from
632 mitochondria requires active caspases and is blocked by Bcl-2. The EMBO Journal. 2001
633 Dec 3;20(23):6627–36.

634 41. Cowling V, Downward J. Caspase-6 is the direct activator of caspase-8 in the cytochrome
635 c -induced apoptosis pathway: absolute requirement for removal of caspase-6
636 prodomain. Cell Death Differ. 2002 Oct;9(10):1046–56.

637 42. Spencer SL, Gaudet S, Albeck JG, Burke JM, Sorger PK. Non-genetic origins of cell-to-cell
638 variability in TRAIL-induced apoptosis. Nature. 2009 May;459(7245):428–32.

639 43. Skilling J. Nested sampling for general Bayesian computation. Bayesian Anal. 2006
640 Dec;1(4):833–59.

641 44. Feroz F, Hobson MP, Bridges M. MultiNest: an efficient and robust Bayesian inference
642 tool for cosmology and particle physics. Mon Not R Astron Soc. 2009 Oct 1;398(4):1601–
643 14.

644 45. Feroz F, Hobson MP, Cameron E, Pettitt AN. Importance Nested Sampling and the
645 MultiNest Algorithm. arXiv:13062144 [astro-ph, physics:physics, stat] [Internet]. 2013 Jun
646 10 [cited 2019 May 14]; Available from: http://arxiv.org/abs/1306.2144

647 46. Buchner J, Georgakakis A, Nandra K, Hsu L, Rangel C, Brightman M, et al. X-ray spectral
648 modelling of the AGN obscuring region in the CDFS: Bayesian model selection and
649 catalogue. A&A. 2014 Apr 1;564:A125.

650 47. Burnham KP, Anderson DR. Model Selection and Multimodel Inference: A Practical
651 Information-Theoretic Approach [Internet]. 2nd ed. New York: Springer-Verlag; 2002
652 [cited 2019 Apr 24]. Available from: https://www.springer.com/us/book/9780387953649

653 48. Symonds MRE, Moussalli A. A brief guide to model selection, multimodel inference and
654 model averaging in behavioural ecology using Akaike's information criterion. Behav Ecol
655 Sociobiol. 2011 Jan 1;65(1):13–21.

656 49. Shockley EM, Rouzer CA, Marnett LJ, Deeds EJ, Lopez CF. Signal integration and
657 information transfer in an allosterically regulated network. npj Syst Biol Appl. 2019 Jul
658 18;5(1):1–9.

659 50. Dai H, Ding H, Peterson KL, Meng XW, Schneider PA, Knorr KLB, et al. Measurement of
660 BH3-only protein tolerance. Cell Death and Differentation. 2018 Jan 1;25(2):282–93.

661 51. Eissing T, Conzelmann H, Gilles ED, Allgöwer F, Bullinger E, Scheurich P. Bistability
662 Analyses of a Caspase Activation Model for Receptor-induced Apoptosis. J Biol Chem.
663 2004 Aug 27;279(35):36892–7.

664 52. Eydgahi H, Chen WW, Muhlich JL, Vitkup D, Tsitsiklis JN, Sorger PK. Properties of cell
665 death models calibrated and compared using Bayesian approaches. Molecular Systems
666 Biology. 2013 Jan 1;9(1):644.

667

53. Aitken S, Akman OE. Nested sampling for parameter inference in systems biology: application to an exemplar circadian model. BMC Systems Biology. 2013 Jul 30;7(1):72.

54. Pullen N, Morris RJ. Bayesian Model Comparison and Parameter Inference in Systems Biology Using Nested Sampling. PLOS ONE. 2014 Feb 11;9(2):e88419.

55. Xu T-R, Vyshemirsky V, Gormand A, Kriegsheim A von, Girolami M, Baillie GS, et al. Inferring Signaling Pathway Topologies from Multiple Perturbation Measurements of Specific Biochemical Species. Sci Signal. 2010 Mar 16;3(113):ra20–ra20.

56. MacKay DJC, Kay DJCM. Information Theory, Inference and Learning Algorithms. Cambridge University Press; 2003. 696 p.

57. Certo M, Moore VDG, Nishino M, Wei G, Korsmeyer S, Armstrong SA, et al. Mitochondria primed by death signals determine cellular addiction to antiapoptotic BCL-2 family members. Cancer Cell. 2006 May 1;9(5):351–65.

58. Burnham KP, Anderson DR. Model Selection and Multimodel Inference: A Practical Information-Theoretic Approach [Internet]. 2nd ed. New York: Springer-Verlag; 2002 [cited 2019 Oct 26]. Available from: https://www.springer.com/gp/book/9780387953649

59. Symonds MRE, Moussalli A. A brief guide to model selection, multimodel inference and model averaging in behavioural ecology using Akaike's information criterion. Behav Ecol Sociobiol. 2011 Jan 1;65(1):13–21.

60. Aldridge BB, Gaudet S, Lauffenburger DA, Sorger PK. Lyapunov exponents and phase diagrams reveal multi-factorial control over TRAIL-induced apoptosis. Molecular Systems Biology. 2011 Jan 1;7(1):553.

61. Handley WJ, Hobson MP, Lasenby AN. PolyChord: next-generation nested sampling. Mon Not R Astron Soc. 2015 Nov 11;453(4):4385–99.

Supporting information

Table S1

Table S2

Table S3

Table S4

Table S5

Table S6

Figures S1-S4

Figures Legends:

Figure 1. **General workflow for the analysis of network dynamics using trends in Bayesian evidence.** The target network is first deconstructed into all relevant subnetworks. A model for each subnetwork and each incrementing set of regulatory conditions is then created and passed to an algorithm for estimation the Bayesian model evidence. The evidence is calculated on a user-defined objective function, describing signal transduction through the network, and over a range of parameter values (the prior). The evidence trends over changing regulatory conditions are then compared to make qualitative inferences regarding network dynamics. In an alternative method, the full model is retained, but the objective function is targeted to different pathways. Inferences on network dynamics can again be made from the trends in the evidence calculations.

Figure 2. Extrinsic apoptosis subnetworks and Bayesian evidence for achieving apoptosis. (A) The direct caspase subnetwork. (B) The direct caspase + mitochondrial activation subnetwork. (C) The direct caspase + mitochondrial inhibition of XIAP subnetwork network. (D) The mitochondrial activation subnetwork. (E) The complete network. (F) the mitochondrial subnetwork. (G) The trends in Bayesian evidence for each of the networks in (A)-(F) over a range of values the apoptosis inhibitor XIAP and for an objective function that computes the proportion of PARP cleavage (a proxy for cell death) at the end of a simulated run.

Figure 3. Evidence values for PARP cleavage and pathway flux at low and high DISC values. (A) Evidence values for PARP cleavage for the caspase pathway and complete network under both low and high DISC conditions (100 and 130,000 molecules per cell of FADD and Caspase-8 respectively). (B) Signal flux through both pathways as well as the total signal flux for high DISC values. (C) Signal flux through both pathways as well as the total signal flux for low DISC values.

Figure 4. Evidence ratio trends under increasing levels of the apoptotic inhibitor XIAP for an inhibited and uninhibited mitochondrial pathway. (A) Evidence trends for the caspase pathway (green), mitochondrial pathway (blue), and complete network (orange) with no MOMP inhibition. (B) Trends for the mitochondria/caspase (blue) and the complete/caspase (orange) evidence ratios from the trends in (A). (C) Evidence trends for the caspase pathway (green), mitochondrial pathway (blue), and complete network (orange) with MOMP inhibitory protein BCL-2 at 328,000 mol. per cell. (D) Trends for the mitochondria/caspase (blue) and the complete/caspase (orange) evidence ratios from the trends in (C).

Figure 5. Precision vs. computational cost. (A) and (B) Average number of evaluations before termination of the MultiNest algorithm over a range of population sizes for the caspase pathway and complete network respectively. (C) and (D) Average of error estimates from MultiNest for each population size and the caspase and complete networks. (E) and (F) Average estimated CPU clock time over each population size for the caspase and complete networks respectively. *MultiNest was unable to estimate the error at XIAP = 0.

738 **Box 1. Extrinsic apoptosis execution.**

739 Extrinsic apoptosis is a receptor mediated process for programmed cell death. The Type I/II phenotypes for the
740 extrinsic apoptosis system were first described by Scaffidi et al. [13]. In that work they examined several cell lines
741 and classified them into those that required the mitochondrial pathway to achieve apoptosis (Type II) and those
742 that don't (Type I). They made several interesting conclusions. They found that Type II cells had relatively weak
743 DISC formation, that both phenotypes responded equally well to receptor mediated cell death, that there was a
744 delay in caspase activation in Type II cells, and that caspase activation happened upstream of mitochondrial
745 activation in Type I cells and downstream in Type II. More recently, XIAP has also been put forth as a critical
746 regulator in the choice of apoptotic phenotype. In Jost et al. [14] they examined hepatocytes (Type II cells) and
747 lymphocytes (Type I cells) under different conditions to examine the role XIAP plays in Type I/II determination.
748 They made several observations upon Fas ligand or Fas-antibody induced apoptosis such as higher levels of XIAP in
749 Type II cells and higher caspase effector activity in XIAP/Bid deficient mice versus apoptosis resistant Bid-only
750 knockouts. In all, they concluded that XIAP is the key regulator that determines the choice of pathway.

751 Extrinsic apoptosis is initiated when a death inducing member of the tumor necrosis factor (TNF) superfamily of
752 receptors (FasR, TNFR1, etc.) is bound by its respective ligand (FasL, TNF-α, etc.), setting off a sequence
753 biochemical events that result in the orderly deconstruction of the cell [15]. The first stage of this sequence is the
754 assembly of the DISC at the cell membrane ① and the subsequent activation of Caspase-8. Upon ligand binding
755 and oligomerization of a receptor such as FasR or TRAIL, an adapter protein, like FADD (Fas-associated protein with
756 death domain), is recruited to the receptors cytoplasmic tail [16, 17, 18]. FADD, in turn, recruits Caspase-8 via their
757 respective death effector domains (DEDs), thus completing DISC formation [17, 18]. Other DISC components could
758 also be included here, such as the regulator cFlip [19]. Once recruited, proximal Procaspase-8 monomers dimerize,
759 inducing their autoproteolytic activity and producing active Caspase-8 [20, 21, 22].

760 After Caspase-8 activation the apoptotic signal can progress down two distinct pathways that both lead to the
761 activation of Caspase-3 and the ensuing proteolysis of downstream targets. One pathway consists of a caspase
762 cascade in which active Caspase-8 directly cleaves and activates Caspase-3 ② [23], while another, more complex
763 pathway is routed through the mitochondria. In the mitochondrial pathway Caspase-8 cleaves the pro-apoptotic
764 Bcl-2 family protein Bid in the cytosol, which then migrates to the mitochondria ③ where it initiates
765 mitochondrial outer membrane permeabilization (MOMP) and the release of pro-apoptotic factors that lead to
766 Caspase-3 activation [24, 25].

767 MOMP has its own set of regulators that govern the strength of apoptotic signaling through the mitochondria ④.
768 After Caspase-8 activated Bid, (tBid), migrates to the mitochondria it activates proteins in the outer mitochondrial
769 membrane, such as Bax, that subsequently self-aggregate into membrane pores and allow exportation of
770 Cytochrome-c and Smac/DIABLO to the cytosol [26]. Bid and Bax are examples of pro-apoptotic proteins from the
771 Bcl-2 family, all of which share BH domain homology [27]. Other members of this family act as MOMP regulators;
772 the anti-apoptotic Bcl-2, for example, binds and inhibits both Bid and Bax while the pro-apoptotic Bad similarly
773 binds and inhibits its target, Bcl-2 [28, 29, 30, 31]. Many other pro- and anti-apoptotic members of the Bcl-2 family
774 have been discovered and together regulate MOMP [32].

775 Regardless of which pathway is chosen, the intermediate results are Caspase-3 activation and subsequent cleavage
776 of PARP ⑧, a proxy for cell death in the analyses here [33, 34]. XIAP (X-linked inhibitor of apoptosis protein) is an
777 inhibitor of Caspase-3 and has been proposed to be a key regulator in determining the Type I/II apoptotic
778 phenotype of a cell [35]. XIAP sequesters Caspase-3 but also contains a ubiquitin ligase domain that directly targets
779 Caspase-3 for degradation. The inhibitor also sequesters and inhibits the Caspase-3 activating Caspase-9 residing
780 within the apoptosome complex [36, 37, 38]. Apoptosome formation is initiated by Cytochrome-c exported from
781 the mitochondria during MOMP ⑤. Cytochrome-c induces the protein APAF-1 to oligomerize and subsequently
782 recruit and activate Caspase-9, thus forming the complex [39]. Another MOMP export, the protein Smac/DIABLO
783 ⑥, binds and inhibits XIAP, working in tandem with Cytochrome-c to oppose XIAP and carry out the apoptosis
784 inducing activity of the Type II pathway [40]. Finally, Procaspase/Caspase-6 constitutes a feed forward loop
785 between Caspase-3 and Caspase-8 ⑦ [41].

786

Figures:

Figure 1.

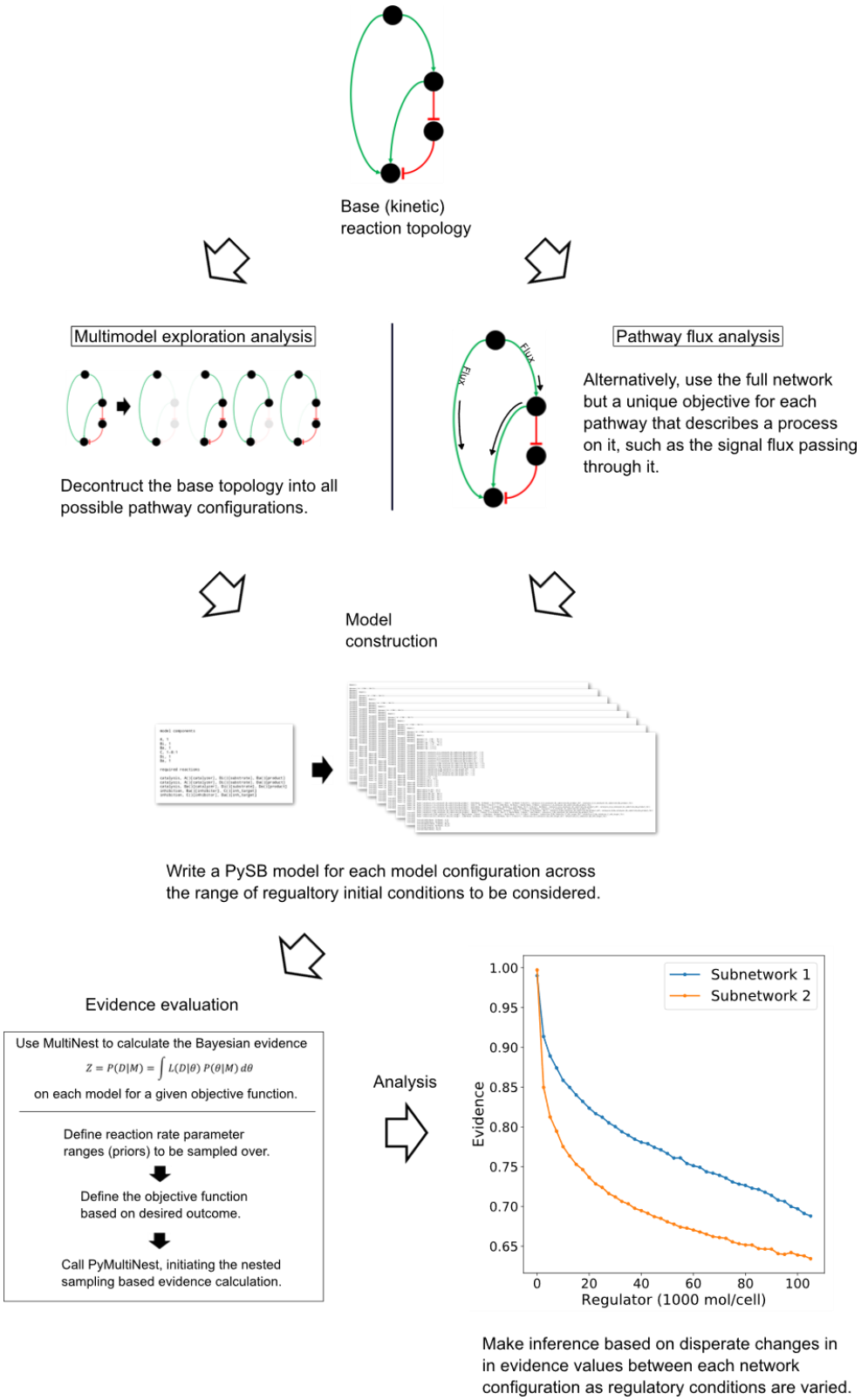

Figure 2.

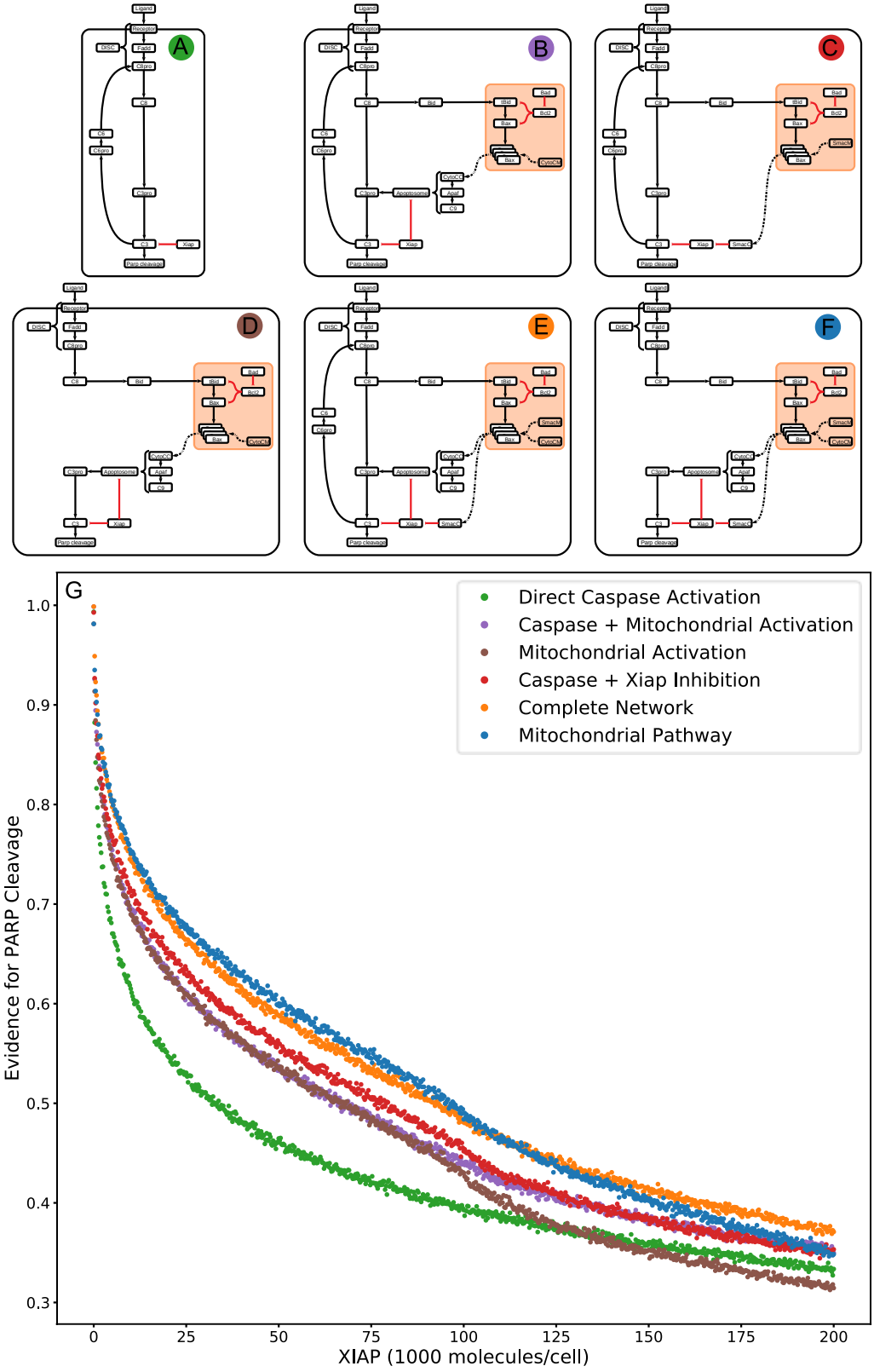
A
B
C
D
E
F
G
Direct Caspase Activation
Caspase + Mitochondrial Activation
Mitochondrial Activation
Caspase + Xiap Inhibition
Complete Network
Mitochondrial Pathway
Evidence for PARP Cleavage
XIAP (1000 molecules/cell)
1.0
0.9
0.8
0.7
0.6
0.5
0.4
0.3
0
25
50
75
100
125
150
175
200

Figure 3.

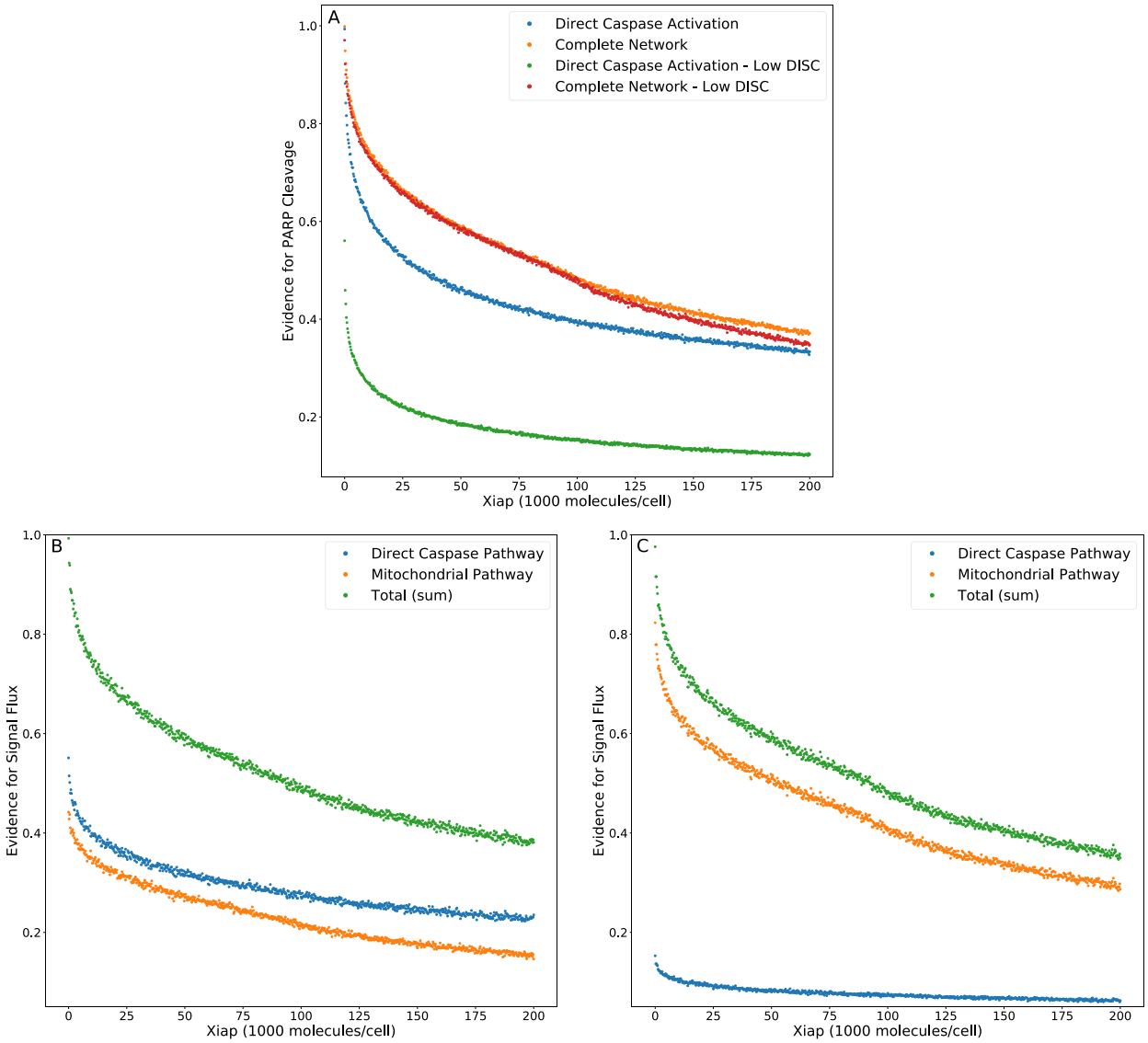
A
Direct Caspase Activation
Complete Network
Direct Caspase Activation - Low DISC
Complete Network - Low DISC
Evidence for PARP Cleavage
Xiap (1000 molecules/cell)
B
Direct Caspase Pathway
Mitochondrial Pathway
Total (sum)
Evidence for Signal Flux
Xiap (1000 molecules/cell)
C
Direct Caspase Pathway
Mitochondrial Pathway
Total (sum)
Evidence for Signal Flux
Xiap (1000 molecules/cell)

Figure 4.

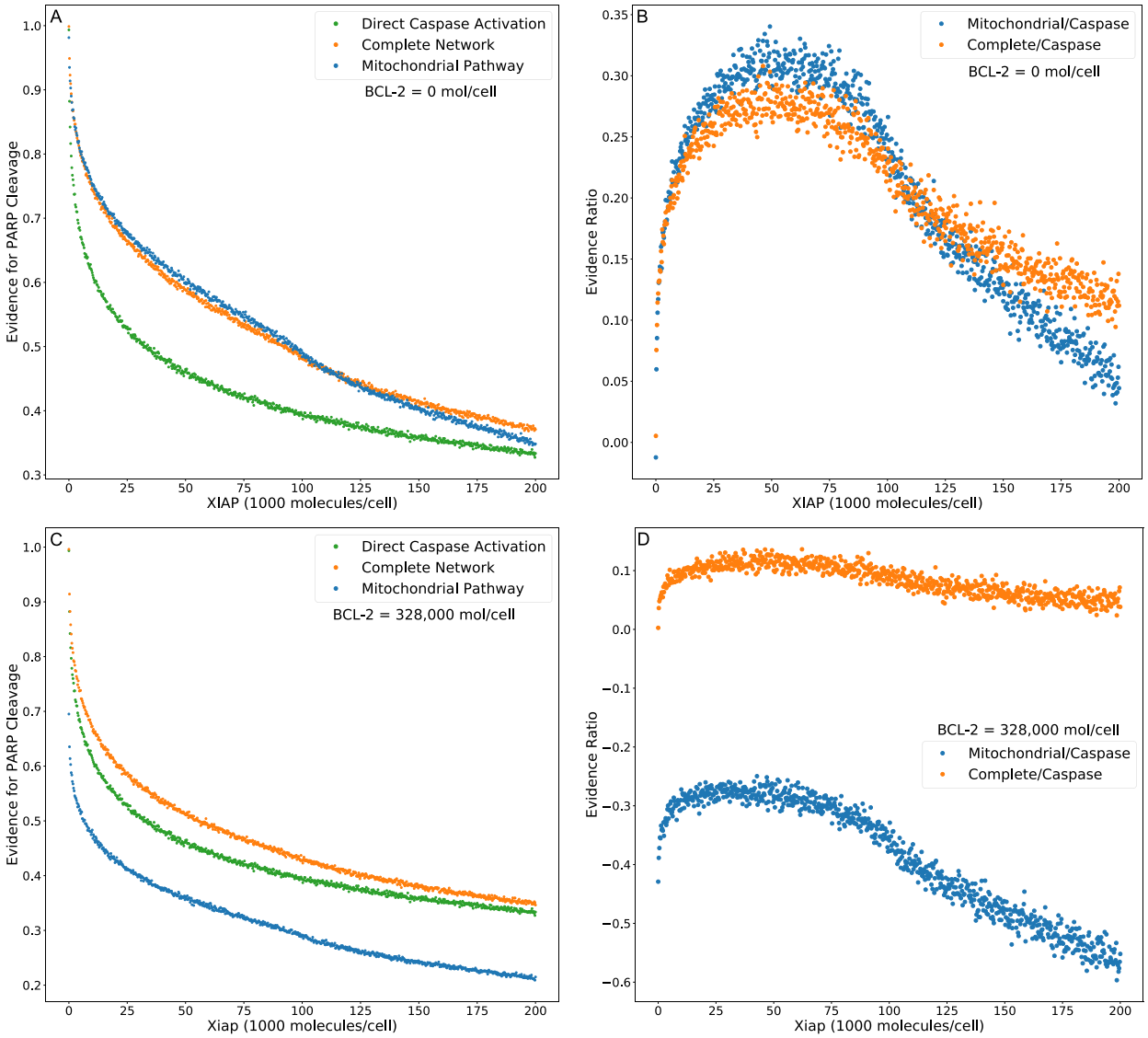
A
Direct Caspase Activation
Complete Network
Mitochondrial Pathway
BCL-2 = 0 mol/cell
Evidence for PARP Cleavage
XIAP (1000 molecules/cell)
B
Mitochondrial/Caspase
Complete/Caspase
BCL-2 = 0 mol/cell
Evidence Ratio
XIAP (1000 molecules/cell)
C
Direct Caspase Activation
Complete Network
Mitochondrial Pathway
BCL-2 = 328,000 mol/cell
Evidence for PARP Cleavage
Xiap (1000 molecules/cell)
D
BCL-2 = 328,000 mol/cell
Mitochondrial/Caspase
Complete/Caspase
Evidence Ratio
Xiap (1000 molecules/cell)

Figure 5.

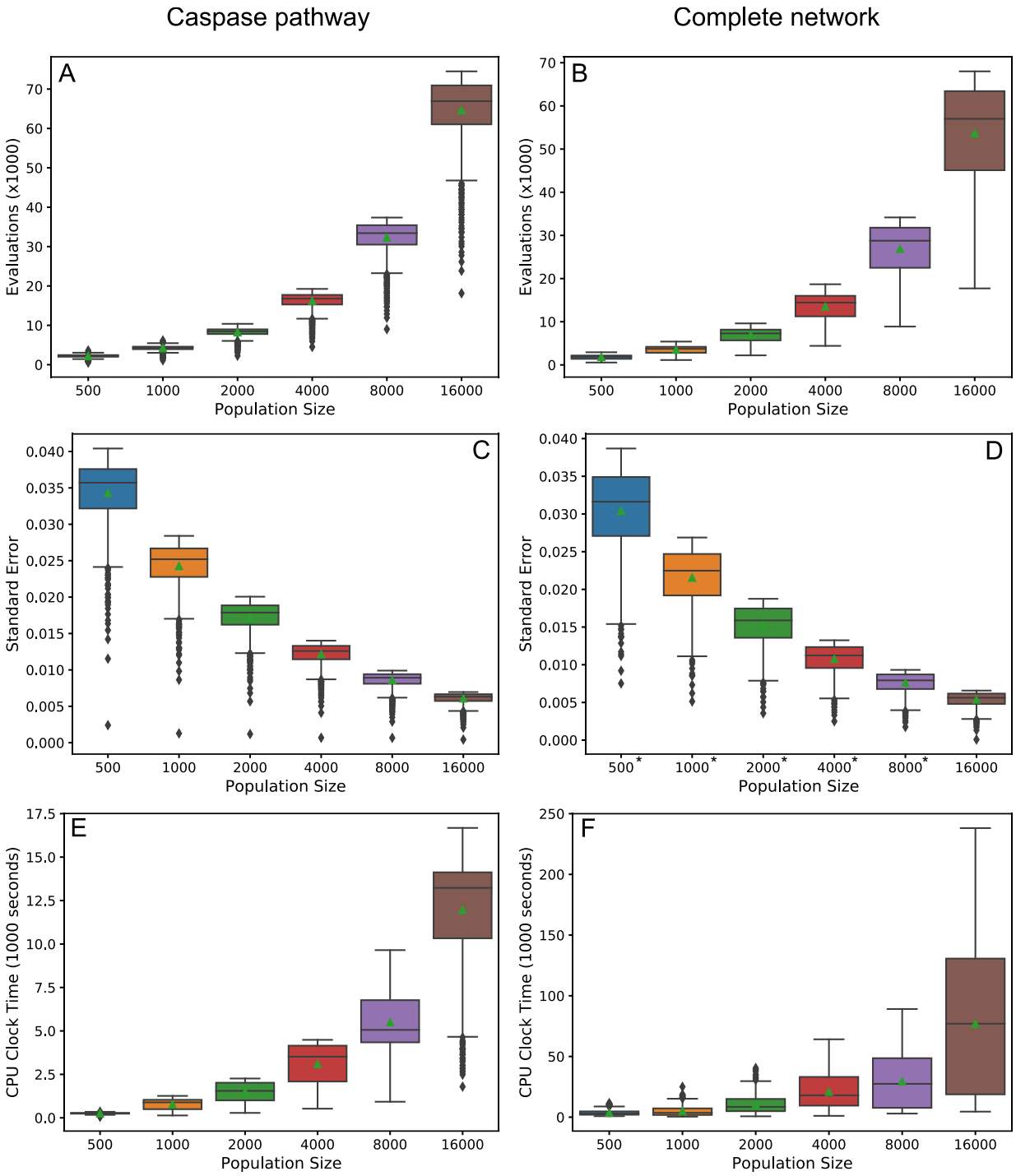
Caspase pathway
Complete network
A
B
C
D
E
F
Evaluations (x1000)
Standard Error
CPU Clock Time (1000 seconds)
Population Size
500
1000
2000
4000
8000
16000
500*
1000*
2000*
4000*
8000*

Box 1.

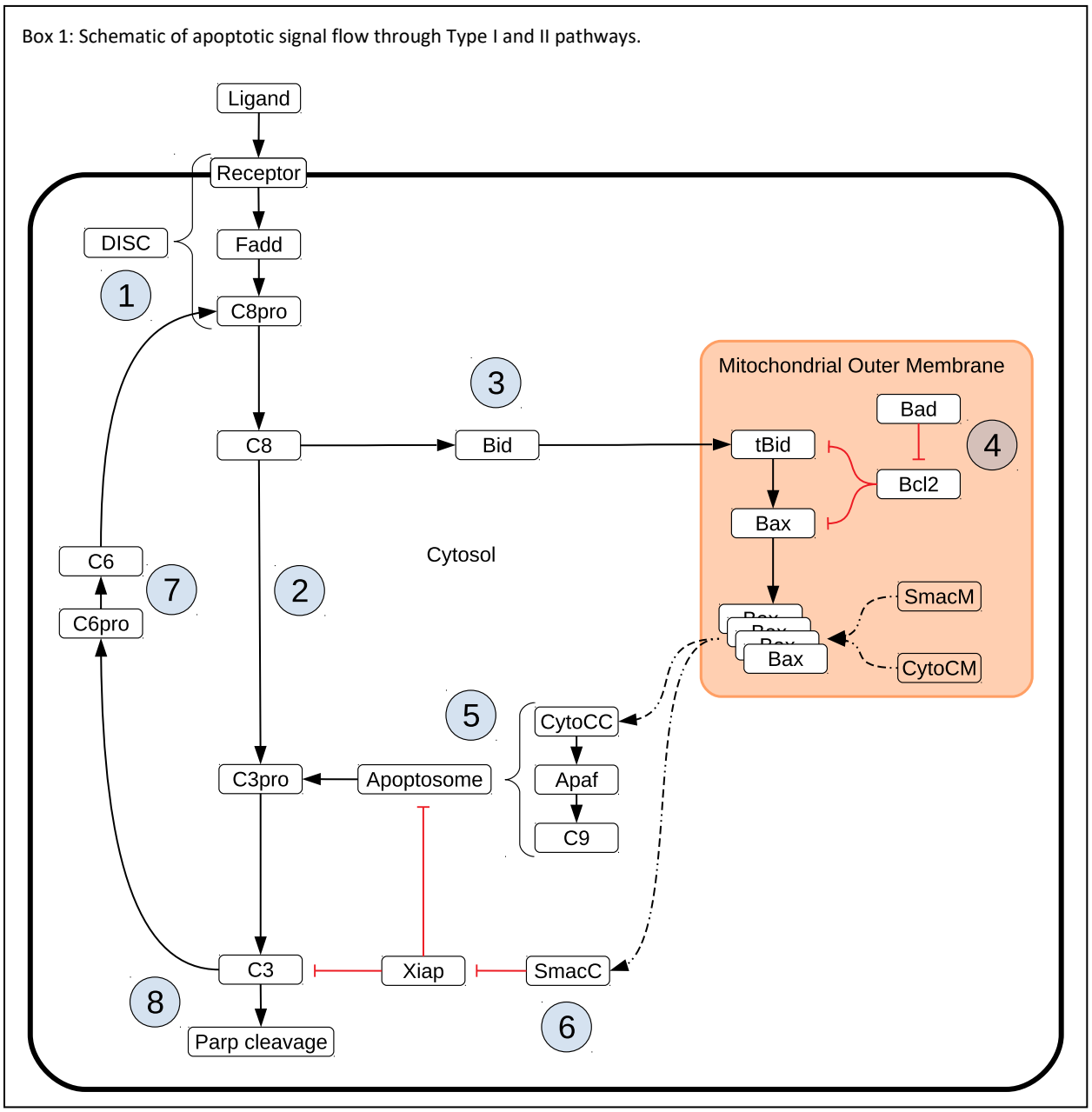
Box 1: Schematic of apoptotic signal flow through Type I and II pathways.
Ligand
Receptor
DISC
Fadd
1
C8pro
3
Mitochondrial Outer Membrane
Bad
C8
Bid
tBid
4
Bcl2
Bax
Cytosol
C6
7
2
SmacM
C6pro
Bax
CytoCM
5
CytoCC
C3pro
Apoptosome
Apaf
C9
C3
Xiap
SmacC
8
6
Parp cleavage